symmetry

MDPI

Article

Durable, Low-Cost, and Efficient Heat Spreader Design from Scrap Aramid Fibers and Hexagonal Boron Nitride

Jung-Hun Yoo [1,2] and Sung Chul Yi [1,3,*]

[1] Department of Chemical Engineering, Hanyang University, 222 Wangsimni ro, Seongdong-gu, Seoul 04763, Republic of Korea
[2] Poongwon Chemical Co., Ltd., 20 Haebong-ro, 255 Beon-gil, Danwon-gu, Ansan 15420, Republic of Korea
[3] Department of Hydrogen and Fuel Cell Technology, Hanyang University, 222 Wangsimni-ro, Seongdong-gu, Seoul 04763, Republic of Korea
* Correspondence: scyi@hanyang.ac.kr

Abstract: Aramid, chemically known as para phenylene terephthalamide or PPD-T, has been widely used in the reinforcement of telecommunication cables, rubber materials (transmission belts, pneumatic belts), ballistic clothing, and frictional materials primarily due to their high tensile resistance, high elastic modulus, and excellent thermal stability (−80–200 °C). These unique properties of aramid originate from its chemical structure, which consists of relatively rigid polymer chains linked by benzene rings and amide bonds (-CO-NH-). Here, in this work inspired by these properties, a heat spreader called Thermal Interface Material (TIM) is developed by synthesizing a resin from scrap aramid fibers. When hexagonal boron nitride (h-BN) as filler is introduced into the as-synthesized aramid resin to form a thin film of thermal sheet (50 µm), an in-plane thermal conductivity as high as 32.973 W/mK is achieved due to the firmly stacked and symmetric arrangement of the h-BN in the resin matrix. Moreover, the influence of h-BN platelet size is studied by fabricating thermal sheets with three different sizes of h-BN (6–7.5 µm, 15–21 µm, and 30–35 µm) in the aramid resin. The results of the study show that as platelet size increases, thermal conductivity increases significantly. Since the resin reported herein is developed out of scrap aramid fibers, the cost involved in the manufacture of the thermal sheet will be greatly lower. As the thermal sheet is designed with h-BN rather than graphene or carbonaceous materials, this high heat spreading sheet can be employed for 5G antenna modules where properties like a low dielectric constant and high electrical insulation are mandated.

Keywords: hexagonal Boron Nitride (h-BN); scrap aramid; heat spreader; TIM

Citation: Yoo, J.-H.; Yi, S.C. Durable, Low-Cost, and Efficient Heat Spreader Design from Scrap Aramid Fibers and Hexagonal Boron Nitride. *Symmetry* **2022**, *14*, 2597. https://doi.org/10.3390/sym14122597

Academic Editor: Raffaele Barretta

Received: 4 November 2022
Accepted: 2 December 2022
Published: 8 December 2022

1. Introduction

New advanced and next-generation technologies such as artificial intelligence, autonomous vehicles, wearable devices, smart cities, wireless technology, and virtual reality are rapidly developing and already impacting life around the globe. Alongside these advancements, another advanced technology essential to all these technologies is 5G communication. Since this fifth generation of mobile network enables high transmission speed, low latency, and hyper-connectivity, it creates a wide range of opportunities in production operations, where latency of even a few microseconds could cause costly disruptions for the manufacturer, and in autonomous vehicle operations, where it facilitates handling the massive data requirements of cellular vehicles. In the telecommunications sector, to contend with the phenomenal growth in data and connectivity, the 5G networks bring in bigger channels for faster data uploads as well as downloads, and also for connecting multiple devices at once [1].

Generally, to maintain a network functioning with such astounding capabilities, 5G technology demands high-power components that utilize lots of energy, and this energy utilization means an immense amount of heat is generated, which can be pernicious to device performance, reliability, and the lifespan of the electronic devices [2]. As far as 5G

mobile devices are concerned, the mobile antenna, chip, and numerous radio units must be housed in a smaller space. This heavy packing density of the components during operation generates uncontrolled heat, and if left unmanaged, electronic components could burn out, resulting in complete breakdown and network failures [3]. Therefore, the true success of the 5G mobile network lies in the efficient thermal management of 5G mmWave antenna modules. Unlike traditional thermal management techniques that use metallic and carbon-based spreaders, 5G mmWave antenna modules require sophisticated heat spreaders made from hexagonal boron nitride (h-BN) because metallic and graphite spreaders are electrically conductive and cause high radio frequency interference [4]. Therefore, this type of h-BN thermal insulation is designed to attach to 5G mmWave antennas for preventing hot spots on the surface with minimal radio frequency interference and for maintaining 5G signal duration to achieve a superior user experience [5–10].

In the manufacture of these specific heat spreaders for 5G mmWave antenna modules, researchers in the field of Thermal Interface Materials (TIMs) prefer two-dimensional h-BN as a filler material over carbon-based material due to the excellent thermal conducting property and low dielectric constant of h-BN [11,12]. For employing it in the thermal management of electronics packaging, h-BN is dispersed in various resin systems, such as SEBS (styrene-ethylene-butylene-styrene), TPU (thermoplastic polyurethane), PI (polyimide), and epoxies as matrix. Some of the notable works that showed decent thermal performance include: (i) Liu et al. developed a composite film of polyimide by blending hexagonal boron nitride with ethyl cellulose ($C_{20}H_{38}O_{11}$) and functionalizing graphene oxide with 2,2′-Bis(trifluoromethyl) benzidine (TFMB- GO). The resulting film, formed with ethyl cellulose, possessed a better thermal conduction network for achieving enhanced thermal conductivity [13] and (ii) Lin Chen et al., using a mussel-inspired approach, functionalized the surface of BN with an infinitesimally thin layer of polydopamine coatings and fabricated a thermal conductivity composite sheet by dispersing the above-mentioned functionalized h-BN in polypropylene (PP) resin. This functionalized BN suppressed phonon scattering and improved thermal conduction by improving filler dispersion and void formation in the PP matrix [14]. Yao et al. reported a highly conductive (thermal) boron nitride/epoxy (BN/EP) composite, wherein hexagonal boron nitrides dispersed in an ethanol solution were filtered by a vacuum pump to form a cake of h-BN. Subsequently, the premade h-BN cake was then infiltrated with a mixture of epoxy monomers (diglycidyl ether of biphenyl-A), curing agent (hexahydro-4-methylphthalic anhydride), and curing accelerator (2, 4, 6-Tris dimethylaminomethyl phenol). The resulting composite sample, after degassing and curing at 100 °C, delivered a thermal conductivity (k) as high as 9 W/mK at a filler concentration of 44 vol% [15]. Similarly, Hsu et al. created polyimide composites with a 30 wt% mixture of micro- and nanosized BN (PI/BN) in a weight ratio of 7:3. It is claimed that the micro-sized BN platelets act as primary channels for thermal passage in composites, whereas the nanosized BN particles serve as a bridge between micro-sized platelets to improve the connectivity of thermal pathways [16]. In a recent study to investigate the effect of pressure on thermal behavior, Moradi et al. developed epoxy-thiol-filled composites with hexagonal BN of sizes 2, 30, and 180 μm. From the experimental results, it is claimed that the application of pressure during curing is found to significantly influence the density and thermal conductivity of the composites, i.e., the enhancement in the thermal conductivity was as a result of improved interfacial interaction between matrix and filler [17,18].

Although a wide range of resin systems are commercially available and have been reported so far (polyolefins [19,20], polypropylene [21], polyethylene [22], poly (vinylidene fluoride) [23], polyphenylene sulfide [24], diglycidylether of bisphenol-A—DGEBA [25], polyurethane [26], polyacrylic resin [27], polyethylene oxide [27], and expanded polystyrene [28,29]) most of them are expensive (Figure 1a), and some show poor flexibility at sufficiently high filler loadings (>60%). Therefore, formulating a cost-effective resin system that is capable of sufficiently dispersing h-BN to make an efficient thermal spreader for 5G antenna modules would be highly desirable [30–33]. In search of an ideal raw material for resin formulation that meets the fundamental criteria of cheaper price, mass producible, good impact resistance,

and flexibility, we landed on one of the lightest and yet extraordinarily strong materials—aramid fabric—for the synthesis of resin solution. The chemical structure of aramid is primarily composed of relatively rigid polymer chains connected by amide bonds (-CO-NH- attached directly to two aromatic rings) and benzene ring structures. The chemical structure of the chain molecules is shaped in such a way that the bonds are aligned along the fiber axis. This structural chemistry of the aramid, together with the strong bonding between relatively short molecules, gives the material its strong tenacity, high modulus, and tremendous toughness. Due to its toughness, flame resistivity, and high strength, it is well-known for its use in defense (stab-resistant vest), the chemical, gas, and electronic sectors [9] (Figure 1b). As these fabrics are used and aged, they become coarse and brittle, losing their effectiveness and providing no protection. Since these weakened industrial and waste fabrics are challenging to recycle, many users prefer either to incinerate them or simply dispose of them in landfills. However, unlike other materials, aramid fabrics are 100% recyclable, and these recycled aramid-derived products can also retain its inherent properties like low flammability, good integrity at higher temperatures, high melting point, and tenacity. Motivated by the promising aspects of recycling aramid fibers, in this work, scrap aramid fibers (aramid from aged product) were utilized in the manufacturing of a cheaper resin system to replace the expensive thermosetting and thermoplastic materials. Since the resin is made from scrap aramid, the developed h-BN/AF thermal spreader is lightweight and possesses excellent strength and good insulation characteristics. Due to the recycling of scrap aramid, this work could not only reduce the amount of discarded aramid from being disposed of in the form of landfilling and incineration but also transform post-industrial aramid waste into a truly sustainable product for electronic thermal management.

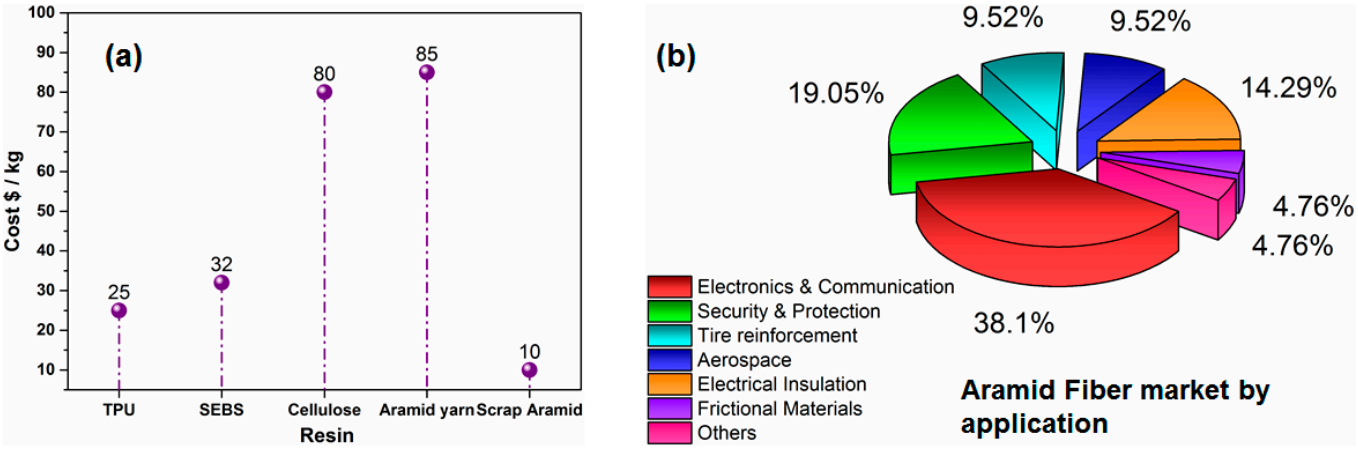

Figure 1. A cost comparison of different resins that are suitable for heat spreader applications (**a**) and a pie chart showing the aramid fiber market by application (**b**).

2. Materials and Method

From discarded impact-resistant panels, aramid fibers were removed and sorted from the products that cannot be recycled. The scrap AF was dissolved in dimethyl sulfoxide (DMSO) in the presence of potassium hydroxide (KOH) under continuous stirring for 72 h (Figure 2). After complete dissolution of AF in the DMSO, h-BN with different wt% was added and stirred for 1 hr. The well-dispersed mixture of AF resin and h-BN filler is then coated into a thin film of thickness 200 µm and immersed immediately in water. The film should remain in water for 4–6 h for a thorough solvent exchange, during which water re-protonates the AF (Figure 3). The hydrogel film was then carefully removed from the water and dried at 80 °C. The dried film was hot pressed for 30 min at 150 tons and 150 °C, resulting in a uniform, flexible, and thin film with a thickness of 40–45 µm. To investigate the effect of h-BN size on the thermal performance, various sizes of h-BN (Figure 4) were procured (CFP-0075: 6–7.5 µm, Haihang: 15–21 µm, and PCTP30: 30–35 µm).

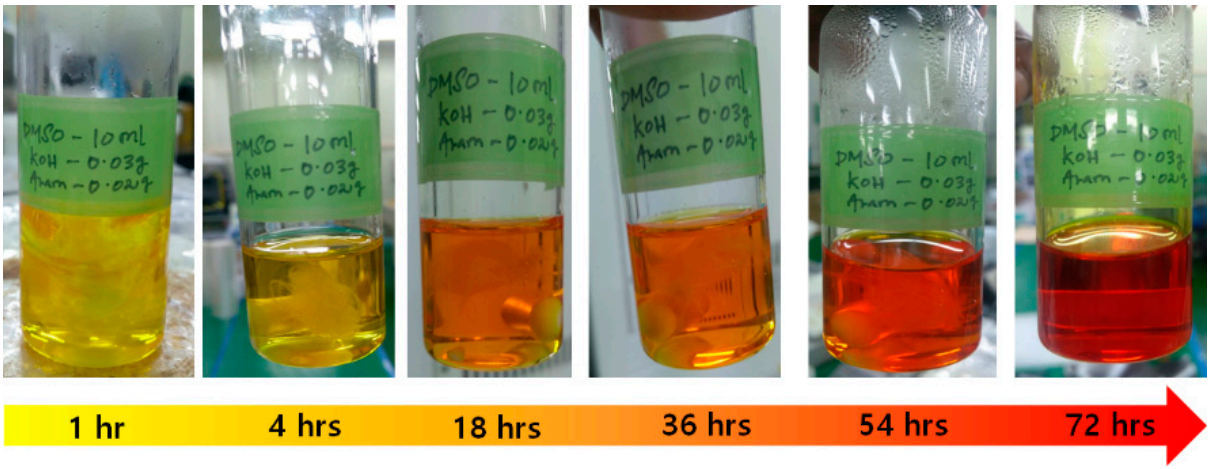

Figure 2. Resin synthesis from waste aramid fibers. Aramid fibers are dissolved in DMSO solvent in the presence of KOH.

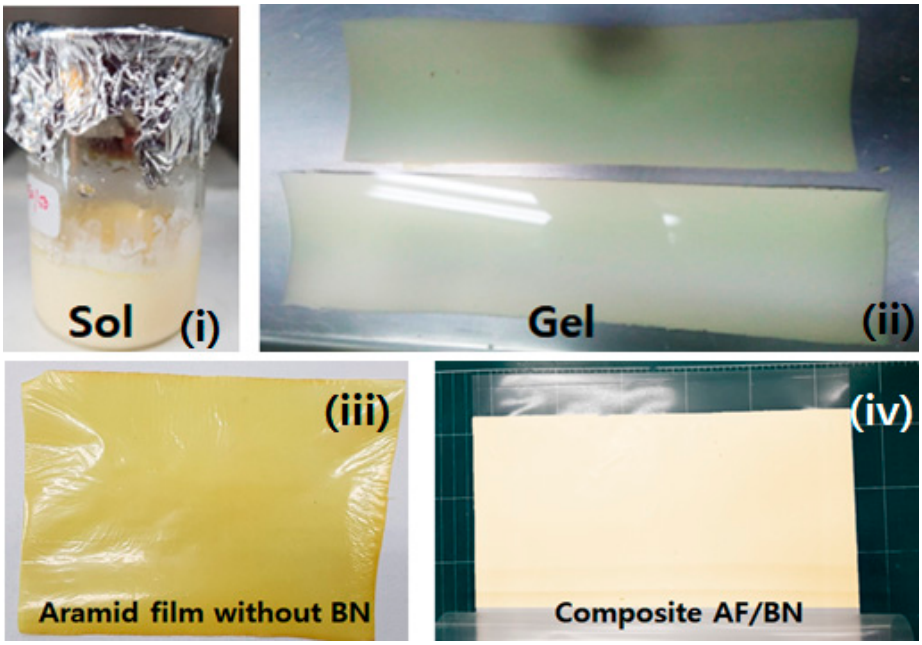

Figure 3. Digital image of aramid/BN sol, film immersed in water for solvent exchange (**i**,**ii**), thermally conductive aramid film with no filler (**iii**), and with h-BN filler (**iv**).

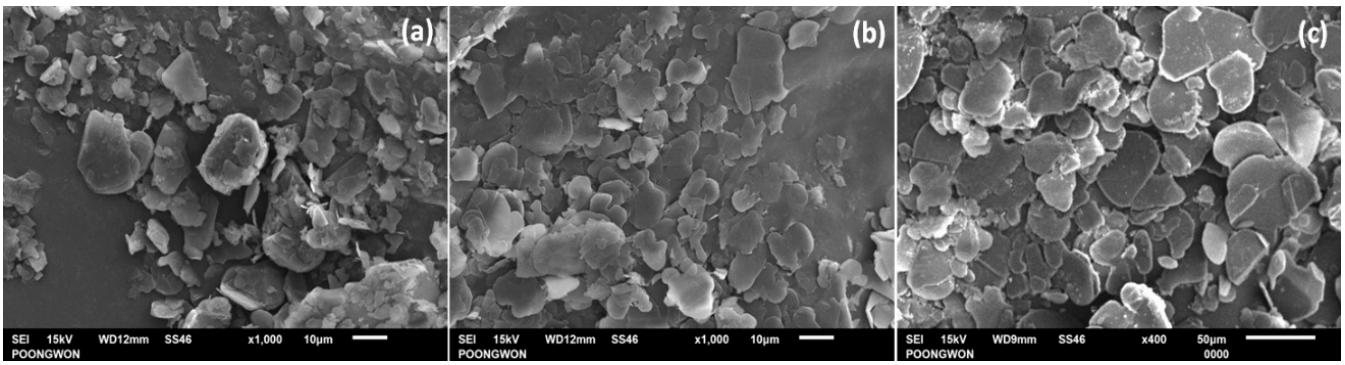

Figure 4. SEM image of three different h-BN used in the study: (**a**) CFP-0075: 6–7.5 μm; (**b**) Haihang: 15–21 μm; and (**c**) PCTP30: 30–35 μm.

3. Characterization

The structure of the (CFP-0075: 6–7.5 μm, Haihang: 15–21 μm, and PCTP30: 30–35 μm) BNs used and the surface morphology of the samples synthesized were identified by field emission scanning electron microscopy (FESEM; JSM-IT700HR, Joel). The thermal properties such as thermal diffusivity—α (mm^2/s), density—ρ (gm/cm^3), and specific heat capacity—C_p (J/g. K) of the fabricated sheets were determined by Laser Flash Analysis (LFA 467, Netzsch), an electronic density meter (ES-E120D), and a Differential Scanning Calorimeter (DSC 241 Polyma, Netzsch), respectively.

4. Results and Discussion

The thermal conductivity '*k*' of the samples was calculated based on the transient thermal analysis method, i.e., temperature is not held constant with respect to time [34]. From the cross-sectional SEM image (Figure 5), the lamellar arrangement of h-BN within the aramid fibers is clearly visible. Since the scrap aramid was dissolved in a DMSO/KOH mixture, the aramid fibers could be broken down to nanofibers, and this nanofibrous aramid form serves as a polymeric building block that offers robust mechanical properties to the BN composite [35–37]. During the hot-press stage, since a high pressure of 150 tons is uniaxially applied, it introduces deliberate orientation of the BN platelets along the horizontal direction. It should be stressed here that, by the application of pressure, not only the majority of the h-BN filler dispersed in aramid resin were horizontally oriented but also the BN platelets were firmly stacked between the aramid fiber networks. The symmetrically layered arrangement of the hexagonal BN within the aramid resin offers an increased number of connections, thereby allowing a seamless path of the thermal network with decreased interfacial resistance [17,38–40]. The surface morphology of the composite samples AF/BN with different h-BN sizes (CFP-0075: 6–7.5 μm, Haihang: 15–21 μm, and PCTP30: 30–35 μm) is illustrated in Figure 5a–c and the uniform distribution of h-BN in the proposed aramid matrix is confirmed from the elemental mapping as shown in Figure 6d–i. Figure 7b,c, shows the in-plane thermal conductivity with respect to filler wt% (Table 1). The loading of h-BN in the aramid solution was increased to 12, 24, 36, 48, and 60 wt%. As anticipated, at the higher filler concentration of 60 wt%, a maximum thermal conductivity of 23.614 W/mK was obtained. The higher the filler content, the greater the thermal conductivity enhancement. However, usually an elevated filler fraction of 60 wt% will severely degrade the mechanical properties like tensile strength, toughness, and flexibility of the thermal spreader. More importantly, during processing, slurries with a higher filler fraction possess higher viscosity and density, subsequently leading to poor coating and dispersibility. Although the sample with a 60 wt% filler concentration showed excellent thermal conductivity, the sample was almost rigid and exhibited poor flexibility, requiring careful handling. Even though the sample at the filler loading of 48 wt% exhibits a 21.45% decrease in the thermal conductivity compared to that of 60 wt%, this optimal loading imparts good flexibility. Therefore, considering the above properties and difficulties during processing, an optimal loading of 40 wt% h-BN is best suited for our proposed aramid resin composite. The samples' C_p with respect to filler loading BN has been identified from differential scanning calorimetry (DSC), and it was determined to be 1.098 J/g.K, 0.915 J/g.K, and 0.807 J/g.K for samples AF with no fillers, AF with 36 wt% h-BN, and AF with 60 wt% h-BN, respectively. The thermal diffusivity of all the samples along the through-plane direction was not significantly higher compared to the in-plane direction, and this can be attributed to the fact that the h-BN, due to its platelet morphology, likely aligns in the direction of resin flow (horizontally), forming effective thermal networks that are favorable for spreading heat. In addition to its heat transfer properties, it is highly advantageous for the heat spreader to show great insulation whenever electric elements are insulated from each other and the ground, and this insulating behavior is obtained by a breakdown voltage test. Our composite samples with h-BNs (CFP-0075: 6–7.5 μm; Haihang: 15–21 μm; and PCTP30: 30–35 μm) dispersed in aramid resin were capable of withstanding a voltage of 1.5–1.8 kV/mm. The proposed thermal sheet, after withstanding this high

voltage, will conduct electricity, and it should be noted that this value is not guaranteed in real-time application over time.

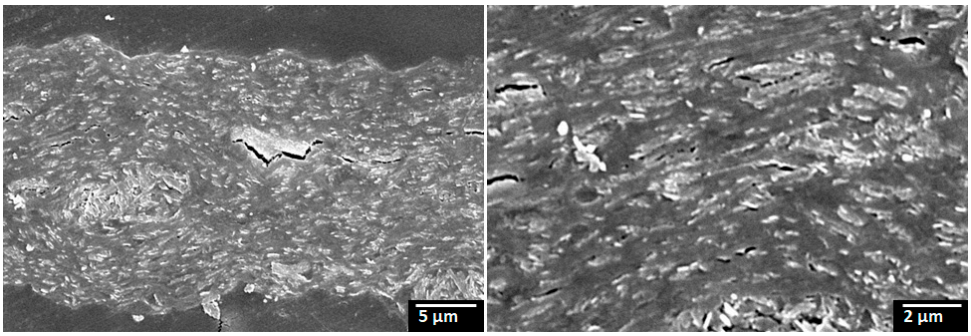

Figure 5. Cross-sectional SEM image of the BN/AF composite.

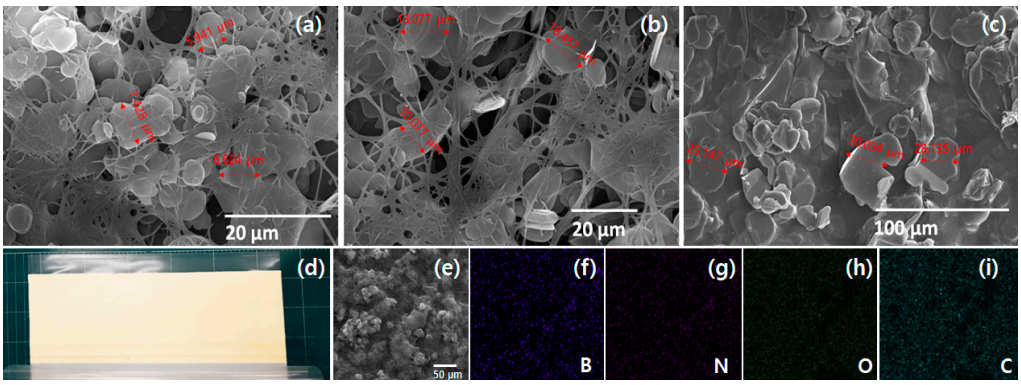

Figure 6. Surface morphology of an AF/BN sample with fillers (**a**) CFP-0075, (**b**) Haihang, (**c**) PCTP30, (**d**) digital image of the AF/BN after hot pressing, and elemental mapping of B, N, C, and O (**e**–**i**).

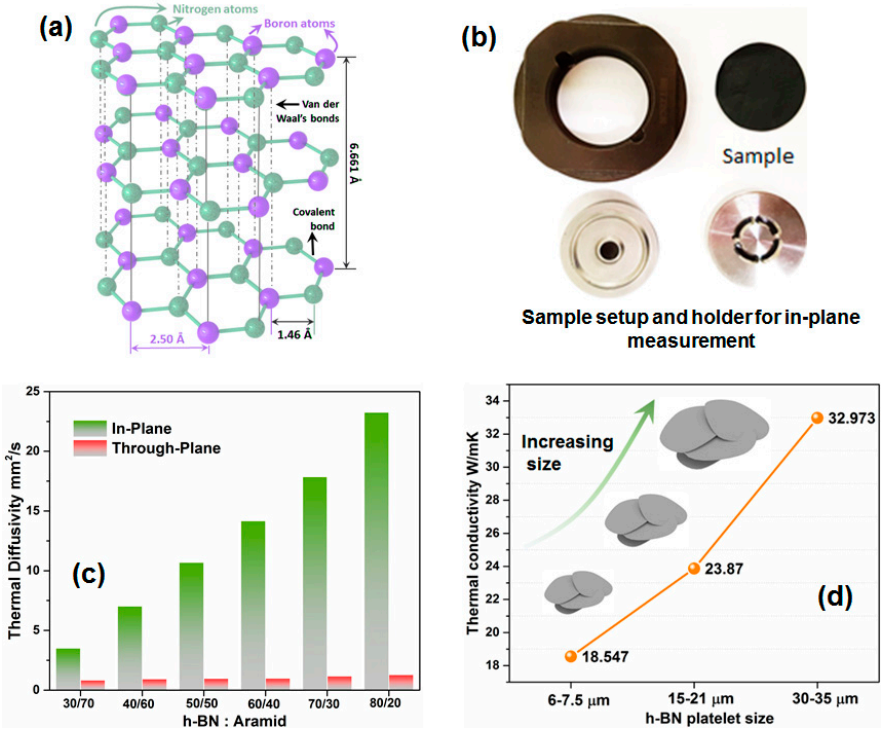

Figure 7. Arrangement of h-BN (**a**), sample setup for in-plane measurement (**b**) [32], thermal behavior of the aramid/h-BN (**c**), and effect of the h-BN size on the thermal performance (**d**).

Table 1. Thermal diffusivity measurement settings are tabulated below [40].

Parameters	Through Plane	In-Plane
Detection size	12.5 mm	24.80 mm
Sample coating	Graphite	Graphite
Voltage	260 V	250 V
Duration	2000 ms	4000 ms
Pulse width	30 µs	50 µs
Main gain	5087	5087

By fixing the filler concentration at 48 wt%, the influence of the size of the h-BN on the thermal performance of the heat spreader was investigated by using fillers of average sizes 6–7.5, 10–15, and ~30 µm. From Figure 7d, it can be observed that as the h-BN size increases, proportionally, the thermal conductivity (in-plane) also increases, suggesting that larger sizes and higher wt.% are more effective towards heat dissipation. It has been found that PCTP30 BN platelets with the size of 30–35 µm delivered the maximum in-plane conductivity of 32.973 W/mK, whereas h-BNs falling under the size range of 6–7.5 µm (0075) and 15–21 µm (Haihang) exhibited a conductivity of 18.547 and 23.870 W/m.K, respectively (Table 2). This is due to the fact that when smaller h-BN fillers are used, interference with thermal transfer will be high, whereas if a larger particle size is employed, a smooth and uninterrupted (with less resistance) heat flow can be achieved. This can be explained theoretically by calculating the interfacial area, which is given by the ratio of area to volume (A/V) of the h-BN:

$$\frac{A}{V} = \frac{2}{t} + \frac{8}{\left(d\sqrt{3}\right)'} \quad (1)$$

where t—thickness (assume t = 0.2 µm) and d—particle size.

Reference BN (CFP-0075), $A/V = 2/0.2 + 8/(7.5\sqrt{3}) = 10.615$ µm^{-1}.

Haihang, $A/V = 2/0.2 + 8/(25\sqrt{3}) = 10.184$ µm^{-1}.

PCTP30, $A/V = 2/0.2 + 8/(35\sqrt{3}) = 10.132$ µm^{-1}.

Table 2. Comparison of the thermal conductivity of the AF/BN with that of other high-loading BN-based composite films.

Composite	k (W/mK)	Reference
f-BNNS/PVA 90/10	4.5	[41]
BN/PVA 57/43	7.47	[42]
f-BNNS/CNF 70/30	30.25	[43]
BNNS/GO 95/5	29.8	[44]
BNNS/GO	11.9	[45]
ANF/BNNS 90/10	2.4	[46]
AF/BN	**32.973**	***This work***

f-BNNS: functionalized BN nanosheets; PVA: poly(vinyl alcohol); ANF: aramid nanofiber; GO: graphene oxide; CNF: cellulose nanofiber.

A lower A/V value suggests a smaller interfacial area, i.e., the larger h-BN (25 µm) provides significantly more continuity for the heat transport in the parallel direction than the smaller h-BN (7.5 µm). The sample, even after 500 bending cycles, retained its thermal conductivity, as only a deviation of 5–6% was observed. From the results of the study, it can be claimed that scrap aramid can be utilized in the manufacture of low cost, durable heat spreaders for TIM applications.

5. Conclusions

By utilizing aramid fibers from scrap, a low-cost resin system is developed for TIM applications. The introduction of h-BN platelets into the aramid resin aided in the formation of thermally conductive channels, while the aramid nanofibers in the resin served as a polymeric building block that offers robust mechanical properties. The study has been extended by investigating the effect of BN platelet size on thermal conductivity. It has been found that PCTP30 BN platelets with the size of 30–35 μm delivered the maximum in-plane conductivity of 32.973 W/mK, whereas h-BNs falling under the size range of 6–7.5 μm (0075) and 15–21 μm (Haihang) exhibited a conductivity of 18.547 and 23.870 W/m.K, respectively. By the process of hot pressing at a sufficiently high pressure of 150 tons, most of the h-BN fillers dispersed in aramid resin were symmetrically and yet horizontally oriented in the aramid fibers, which allowed for a seamless path of the thermal network. However, given the promising thermal performance of the sheet made from scrap aramid, the current work also highlights the feasibility of recycling discarded fiber waste for thermal management applications.

Author Contributions: Conceptualization, J.-H.Y. and S.C.Y.; methodology, S.C.Y.; software, J.-H.Y.; validation, J.-H.Y., S.C.Y.; formal analysis, J.-H.Y.; investigation, S.C.Y.; resources, J.-H.Y.; data curation, J.-H.Y.; writing—original draft preparation, J.-H.Y.; writing—review and editing, S.C.Y.; visualization, S.C.Y.; supervision, S.C.Y.; project administration, S.C.Y.; funding acquisition, J.-H.Y. All authors have read and agreed to the published version of the manuscript.

Funding: The work was supported by the Korea Evaluation Institute of Industrial Technology (Grant No. 20000479). Assistance provided by study participants and team members of Thermal Interface Materials, Poongwon Chemicals, was greatly appreciated.

Institutional Review Board Statement: Not applicable.

Informed Consent Statement: Not applicable.

Data Availability Statement: Not applicable.

Conflicts of Interest: The authors declare no conflict of interest.

References

1. Kitahara, H.; Oku, T. Nanostructures and electronic properties of carbon and boron nitride nanocapsules. *J. Ceram. Process. Res.* **2004**, *5*, 89–93.
2. Alazzam, M.B.; Hajjej, F.; AlGhamdi, A.S.; Ayouni, S.; Rahman, M.A. Mechanics of materials natural fibers technology on thermal properties of polymer. *Adv. Mater. Sci. Eng.* **2022**, *2022*, 1–5. [CrossRef]
3. Kugimoto, H.; Uehara, M.; Enomoto, N.; Hojo, J. Rod-like Si3N4 grain growth in the sintered body of amorphous Si3N4-BN composite powder with sintering additives. *J. Ceram. Process. Res.* **2003**, *4*, 6–9.
4. Kim, D.; Lee, Y.; Chacón, A.; Kim, D.-E. Effect of interlayer coupling and symmetry on high-order harmonic generation from monolayer and bilayer hexagonal boron nitride. *Symmetry* **2022**, *14*, 84. [CrossRef]
5. Besisa, D.H.; Hagras, M.A.; Ewais, E.M.; Ahmed, Y.M.; Zaki, Z.I.; Ahmed, A.J. Low temperature synthesis of nano-crystalline h-boron nitride from boric acid/urea precursors. *J. Ceram. Process. Researc.* **2016**, *17*, 1219–1225.
6. Fu, L.; Wang, T.; Yu, J.; Dai, W.; Sun, H.; Liu, Z.; Sun, R.; Jiang, N.; Yu, A.; Lin, C.-T. An ultrathin high-performance heat spreader fabricated with hydroxylated boron nitride nanosheets. *J. 2D Mater.* **2017**, *4*, 025047. [CrossRef]
7. Chen, H.; Ginzburg, V.V.; Yang, J.; Yang, Y.; Liu, W.; Huang, Y.; Du, L.; Chen, B. Thermal conductivity of polymer-based composites: Fundamentals and applications. *Prog. Polym. Sci.* **2016**, *59*, 41–85. [CrossRef]
8. Lim, C.S.; Ryu, J.H.; Kim, D.-H.; Cho, S.-Y.; Oh, W.-C. Reaction morphology and the effect of pH on the preparation of TiO2 nanoparticles by a sol-gel method. *J. Ceram. Process. Res.* **2010**, *11*, 736–741.
9. Wang, Y.; Xia, S.; Xiao, G.; Di, J.; Wang, J. High-loading boron nitride-based bio-inspired paper with plastic-like ductility and metal-like thermal conductivity. *ACS Appl. Mater. Interfaces* **2020**, *12*, 13156–13164. [CrossRef]
10. Švec, P.J. Microstructure and mechanical properties of B4C-TiB2 ceramic composites hot pressed with in-situ reaction. *J. Ceram. Process. Res.* **2019**, *20*, 113–120. [CrossRef]
11. Zhong, J.; Feng, Y.; Wang, H.; Hu, D. Fabrication and characterization of hexagonal boron nitride powder by a precursor conversion method. *J. Ceram. Process. Res.* **2013**, *14*, 269–273.
12. Ning, Z.; Huan, L.; Tianwen, Z.; Hongmin, K.; Xiaoyang, W.; Xingyu, C. Effects of boron source composition ratio on the microstructure and adsorption performance of hexagonal boron nitride prepared by template method. *J. Ceram. Process. Res.* **2016**, *17*, 181–185.

13. Liu, L.; Shen, S.; Wang, Y. Enhanced thermal conductivity of flexible h-BN/polyimide composites films with ethyl cellulose. *e-Polymers* **2019**, *19*, 305–312. [CrossRef]
14. Chen, L.; Xu, H.-F.; He, S.-J.; Du, Y.-H.; Yu, N.-J.; Du, X.-Z.; Lin, J.; Nazarenko, S. Thermal conductivity performance of polypropylene composites filled with polydopamine-functionalized hexagonal boron nitride. *PLoS ONE* **2017**, *12*, e0170523. [CrossRef] [PubMed]
15. Sayam, A.; Rahman, A.; Rahman, M.; Smriti, S.A.; Ahmed, F.; Rabbi, M.; Hossain, M.; Faruque, M. A review on carbon fiber-reinforced hierarchical composites: Mechanical performance, manufacturing process, structural applications and allied challenges. *Carbon Lett.* **2022**, *32*, 1–33. [CrossRef]
16. Li, T.-L.; Hsu, S.L.-C. Enhanced thermal conductivity of polyimide films via a hybrid of micro-and nano-sized boron nitride. *J. Phys. Chem. B* **2010**, *114*, 6825–6829. [CrossRef]
17. Moradi, S.; Román, F.; Calventus, Y.; Hutchinson, J. Remarkable Thermal Conductivity of Epoxy Composites Filled with Boron Nitride and Cured under Pressure. *Polymers* **2021**, *13*, 955. [CrossRef]
18. Pramono, A.E.; Nura, M.Z.; Soedarsonob, J.; Indayaningsih, N. Properties of wear rate and electrical conductivity of carbon ceramic composites. *J. Ceram. Process. Res.* **2019**, *20*, 1–7. [CrossRef]
19. Antunes, M.; Realinho, V.; Velasco, J.I.; Solórzano, E.; Rodríguez-Pérez, M.-Á.; de Saja, J.A. Thermal conductivity anisotropy in polypropylene foams prepared by supercritical CO_2 dissolution. *Mater. Chem. Phys.* **2012**, *136*, 268–276. [CrossRef]
20. Ferreira, F.; Franceschi, W.; Menezes, B.; Brito, F.; Lozano, K.; Coutinho, A.; Cividanes, L.; Thim, G. Dodecylamine functionalization of carbon nanotubes to improve dispersion, thermal and mechanical properties of polyethylene based nanocomposites. *Appl. Surf. Sci.* **2017**, *410*, 267–277. [CrossRef]
21. Muratov, D.; Kuznetsov, D.; Il'Inykh, I.; Mazov, I.; Stepashkin, A.; Tcherdyntsev, V. Thermal conductivity of polypropylene filled with inorganic particles. *J. Alloy. Compd.* **2014**, *586*, S451–S454. [CrossRef]
22. Yang, C.; Navarro, M.; Zhao, B.; Leng, G.; Xu, G.; Wang, L.; Jin, Y.; Ding, Y. Thermal conductivity enhancement of recycled high density polyethylene as a storage media for latent heat thermal energy storage. *Sol. Energy Mater. Sol. Cells* **2016**, *152*, 103–110. [CrossRef]
23. Cao, J.-P.; Zhao, J.; Zhao, X.; You, F.; Yu, H.; Hu, G.-H.; Dang, Z.-M. High thermal conductivity and high electrical resistivity of poly (vinylidene fluoride)/polystyrene blends by controlling the localization of hybrid fillers. *Compos. Sci. Technol.* **2013**, *89*, 142–148. [CrossRef]
24. Guo, Y.; Ruan, K.; Shi, X.; Yang, X.; Gu, J. Factors affecting thermal conductivities of the polymers and polymer composites: A review. *Compos. Sci. Technol.* **2020**, *193*, 108134. [CrossRef]
25. Kiran, V.; Gaur, B. Curing and thermal behavior of epoxy resins of hexafluoro-bisphenol–A and bisphenol-A. *Polímeros* **2016**, *26*, 11–20. [CrossRef]
26. Messina, E.; Leone, N.; Foti, A.; Di Marco, G.; Riccucci, C.; Di Carlo, G.; Di Maggio, F.; Cassata, A.; Gargano, L.; D'Andrea, C. Double-wall nanotubes and graphene nanoplatelets for hybrid conductive adhesives with enhanced thermal and electrical conductivity. *ACS Appl. Mater. Interfaces* **2016**, *8*, 23244–23259. [CrossRef] [PubMed]
27. Singh, A.K.; Panda, B.P.; Mohanty, S.; Nayak, S.K.; Gupta, M.K. Recent developments on epoxy-based thermally conductive adhesives (TCA): A review. *Polym.-Plast. Technol. Eng.* **2018**, *57*, 903–934. [CrossRef]
28. Liu, B.; Li, Y.; Fei, T.; Han, S.; Xia, C.; Shan, Z.; Jiang, J. Highly thermally conductive polystyrene/polypropylene/boron nitride composites with 3D segregated structure prepared by solution-mixing and hot-pressing method. *Chem. Eng. J.* **2020**, *385*, 123829. [CrossRef]
29. Mrajji, O.; El Wazna, M.; Ouhaibi, S.; Sair, S.; El Bouari, A.; Cherkaoui, O.; Belouaggadia, N. *Thermal Performance of Building Materials Based on Feather and Polystyrene Wastes*; IOP Conference Series: Materials Science and Engineering; IOP Publishing: Bristol, UK, 2020; p. 012010.
30. Souza, M.K.; Lima, E.P.; Nascimento, I.V.; Montazerian, M.; Baino, F.; Fook, M.V. Development, characterization and optimization of a new bone cement based on calcium–Strontium aluminates and chitosan-glycerin solution. *Ceram. Int.* **2022**, *48*, 31866–31879. [CrossRef]
31. Uher, C. Thermal conductivity of high-T c superconductors. *J. Supercond.* **1990**, *3*, 337–389. [CrossRef]
32. Burger, N.; Laachachi, A.; Ferriol, M.; Lutz, M.; Toniazzo, V.; Ruch, D. Review of thermal conductivity in composites: Mechanisms, parameters and theory. *Prog. Polym. Sci.* **2016**, *61*, 1–28. [CrossRef]
33. Zhai, S.; Zhang, P.; Xian, Y.; Zeng, J.; Shi, B. Effective thermal conductivity of polymer composites: Theoretical models and simulation models. *Int. J. Heat Mass Transf.* **2018**, *117*, 358–374. [CrossRef]
34. Shimizu, Y.; Ishii, J.; Shinzato, K.; Baba, T. A novel method for determination of the thermal diffusivity of thin films using a modulated CO_2 laser. *Int. J. Thermophys.* **2005**, *26*, 203–211. [CrossRef]
35. Yang, M.; Cao, K.; Sui, L.; Qi, Y.; Zhu, J.; Waas, A.; Arruda, E.M.; Kieffer, J.; Thouless, M.; Kotov, N.A. Dispersions of aramid nanofibers: A new nanoscale building block. *ACS Nano* **2011**, *5*, 6945–6954. [CrossRef]
36. Hammer, C. Cooperative molecular motion in blends of poly (vinyl chloride) with ethylene-vinyl acetate copolymers. *Macromolecules* **1971**, *4*, 69–71. [CrossRef]
37. ATALA, M.; GÜL AYGÜN, E.; Doğan, A. Evaluation of the crack formation of feldspathic ceramic reinforced with bor chemicals. *J. Ceram. Process. Res.* **2020**, *21*, 407–415.

38. Liu, Z.; Li, J.; Liu, X. Novel functionalized BN nanosheets/epoxy composites with advanced thermal conductivity and mechanical properties. *ACS Appl. Mater. Interfaces* **2020**, *12*, 6503–6515. [CrossRef]
39. Kim, H.; Jeon, D.-Y.; Jang, S.G.; Lee, M.W. Synergetic effect of BN for the electrical conductivity of CNT/PAN composite fiber. *J. Mech. Sci. Technol.* **2022**, *36*, 3103–3107. [CrossRef]
40. Yoo, J.-H.; Maiyalagan, T.; Yi, S.C. Thermal conductive thin, flexible composite sheet of boron nitride aggregates and alumina for enhanced through plane conductivity. *Ceram. Int.* **2022**, *48*, 29183–29189. [CrossRef]
41. Chen, Y.; Zhang, H.; Chen, J.; Guo, Y.; Jiang, P.; Gao, F.; Bao, H.; Huang, X. Thermally Conductive but Electrically Insulating Polybenzazole Nanofiber/Boron Nitride Nanosheets Nanocomposite Paper for Heat Dissipation of 5G Base Stations and Transformers. *ACS Nano* **2022**, *16*, 14323–14333. [CrossRef]
42. Yin, C.-G.; Liu, Z.-J.; Mo, R.; Fan, J.-C.; Shi, P.-H.; Xu, Q.-J.; Min, Y.-L. Copper nanowires embedded in boron nitride nanosheet-polymer composites with enhanced thermal conductivities for thermal management. *Polymer* **2020**, *195*, 122455. [CrossRef]
43. Wu, K.; Fang, J.; Ma, J.; Huang, R.; Chai, S.; Chen, F.; Fu, Q. Achieving a Collapsible, Strong, and Highly Thermally Conductive Film Based on Oriented Functionalized Boron Nitride Nanosheets and Cellulose Nanofiber. *ACS Appl. Mater. Interfaces* **2017**, *9*, 30035–30045. [CrossRef] [PubMed]
44. Yao, Y.; Zeng, X.; Wang, F.; Sun, R.; Xu, J.-b.; Wong, C.-P. Significant Enhancement of Thermal Conductivity in Bioinspired Freestanding Boron Nitride Papers Filled with Graphene Oxide. *Chem. Mater.* **2016**, *28*, 1049–1057. [CrossRef]
45. Li, P.; Shen, H.; Qian, Z.; Yang, X.; Zhao, N.; Zhu, C.; Xu, J. Facile fabrication of flexible layered GO/BNNS composite films with high thermal conductivity. *J. Mater. Sci.* **2018**, *53*, 4189–4198. [CrossRef]
46. Rahman, M.M.; Puthirath, A.B.; Adumbumkulath, A.; Tsafack, T.; Robatjazi, H.; Barnes, M.; Wang, Z.; Kommandur, S.; Susarla, S.; Sajadi, S.M.; et al. Fiber reinforced layered dielectric nanocomposite. *Adv. Funct. Mater.* **2019**, *29*, 1900056. [CrossRef]